Compact modeling of the switching dynamics and temperature dependencies in TiOx memristors: Part II - Physics Based Model

Dhirendra Vaidya, Shraddha Kothari, Thomas Abbey, Spyros Stathopoulos, Loukas Michalas, Alexantrou Serb and Themis Prodromakis

***Abstract*—In the second part of this series, we propose a physics-based model for describing the temperature dependence of TiO_x based memristors, both switching and static. We show that, current-voltage (I-V) characteristics of memristor in the non-switching regime, indicating a Schottky emission mechanism, can be described by minor modifications to the Schottky current equation. This leads to a physics-based static I-V compact model. Simultaneously, we show that, the temperature dependence of the switching dynamics model parameters naturally emerges as a mere scaling factor from the static I-V model. This is a computationally efficient approach which does not require any additional parameters to extend the switching dynamics model for incorporating thermal dependence.**

***Index Terms*—Metal oxide memristors, TiO_x memristors, resistive RAMs, compact model, switching dynamics, static I-V, Schottky emission, temperature dependence, pulsed resistance transient measurements, physics based model**

I. Introduction

TiO_x has been shown to be one of the most promising oxide materials for memristive devices [1], [2], [3], [4], [5], [6], [7]. It is a CMOS-compatible material that can be used to realise high density arrays of memristor devices [8], [9]. In this part of the series we focus on TiO_x memristors which have been shown to exhibit Schottky emission [5], [10] as the dominant conduction mechanism in low-field regime. These devices exhibit following operating modes: (1) a sub-threshold 'non-switching' or 'static' regime and (2) a supra-threshold 'switching regime'. Switching and static regimes can be best understood from Fig. 1 which shows current-voltage characteristics of a Pt/TiO_x/Pt memristor. When the I-V is traced only up to ± 0.5 V, no hysteresis is observed, however for higher biases i.e. $|V| > 0.5$ V a hysteresis loop can be seen indicating resistive switching. For memory applications of memristors, a bias in the non-switching regime can be used for read operation whereas a bias in the switching regime can be used for set/reset operations.

Strukov et. al [1] have used simple linear relationship to describe the I-V characteristics of memristor devices. However, in reality memristor I-V characterisitcs can exhibit non-linear behaviour. Simmon's tunneling barrier model [11] has been one of the most widely used models for metal-insulator-metal (MIM) memristors [12], [13], [14], [15]. However, the expected temperature sensitivity of I-V characteristics in tunnelling-based conduction mechanisms is weak. In TiO_x-based devices, however, a significant thermal sensitivity has been observed [10], [16], revealing a barrier controlled conduction mechanism, i.e. Schottky emission in metal/TiO_x/metal memristors. For this reason we use the Schottky current equation instead of Simmon's tunnel barrier model to describe static I-V characteristics.

In this paper, we propose a physics-based, compact model for describing the static I-V characteristics of memrsitive devices. The model is based on the Schottky current equation with minor modifications to improve accuracy. We then proceed to use static I-V and pulsed resistance transient (PRT) testing protocols to measure the electrical characteristics of TiO_x memristors at a range of temperatures. Finally, we attempt to predict how the resistive switching behaviour changes purely as a result of applying the Schottky barrier temperature correction factor on the baseline model and conclude that this modification may be sufficient to explain all observed thermally-induced variations in resistive switching. This is significant because: i) it shows that to a good approximation to the thermal dependence of resistive switching is grounded entirely on the effect of temperature on the static I-V (i.e. the actual process of resistive switching itself is effectively temperature-independent) and ii) it allows for a very compact way of modelling thermal effects on both static and dynamic electrical characteristics of our memristive devices.

II. Experimental methods

The experimental data presented in this work is obtained from two specimens of TiO_x memristors referred to as memristor I-b and memristor II in part I as well as in part II of the series. For memristor I-b (for memristor II), both the top and bottom electrodes are deposited using e-beam evaporation technique. The bottom electrode comprises of 12 nm Pt (20 nm Au) and 5 nm Ti, of which Ti is used as an adhesive layer between oxidized Si substrate and the Pt layer. In both the types of memristor devices top electrode is Pt (15 nm for memristor I-b and 12 nm for memristor II). For memristor I-b (memristor II) 10 nm (25 nm) TiO_x active layer is deposited at room temperature using magnetron sputtering. Further details of the fabrication technique can be found in part I of the series. The memristors are electroformed using an incremental step pulse train protocol, identical to part I of the series.

The authors are with the Centre for Electronics Frontiers, University of Southampton, Southampton, SO171BJ, UK (e-mail: dhirendra22121987@gmail.com, t.prodromakis@soton.ac.uk)

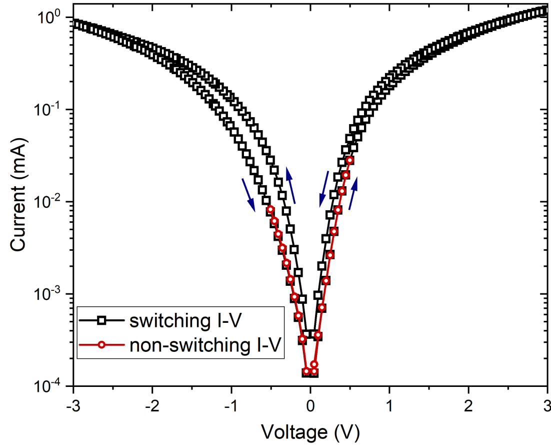

Fig. 1. A pair of I-V curves from a Pt/TiO_x/Pt memristor device. When the I-V is traced only up to ±0.5 V, hysteresis is absent, indicating no resistive switching at any point along the trajectory. In contrast, when an I-V is traced to ±3 V, hysteresis is observed indicating a change in device resistance.

For electrical characterisation we use Arc One from Arc Instruments [17], [18]. Static I-V characteristics are obtained by sweeping the pulse amplitude. In the static I-V measurements pulse width and inter-pulse off-time both are fixed at 10 ms. Similar to part I, PRT measurements are also obtained using Arc One from Arc Instruments [17]. For the temperature dependence measurements for memristor I-b, we use a chuck-based temperature controller which is suitable for devices on wafer. This approach is different from the micro-chamber based temperature controller [19] used for memristor II (which is suitable for packaged devices). Suitable thermal settling times were allowed in order to ensure that chip temperature converged in both set-ups.

III. Static I-V Model

For TiO_x memristors it was shown that carrier transport is barrier controlled [10] and the dominant mechanism in the non-switching regime is Schottky emission, which is described as:

$$I = AA^{*}T^{2}\exp\left(-\frac{q(\phi_B - \alpha\sqrt{V})}{k_B T}\right) \tag{1}$$

where, I is measured current, V is applied bias across top and bottom electrodes, T is temperature, ϕ_B is Schottky barrier height, α is Schottky barrier lowering factor, k_B is the Boltzmann constant, A is device area and A^* is the Richardson's constant. Note that, in eq. (1), Richardson constant A^* and Schottky barrier lowering factor α in general can have a temperature dependence. A^*, α and ϕ_B can be extracted (or fitted) using temperature dependent I-V measurements. For the purpose of compact modelling, the temperature dependence of Richardson's constant can be accounted by modifying the Schottky current equation to,

$$I = AA_m^{*}T^{C_T}\exp\left(-\frac{q(\phi_B - \alpha\sqrt{V})}{k_B T}\right) \tag{2}$$

Eq. (2) introduces more fitting parameters, C_T, and A_m^*. A_m^* is temperature independent and referred to as modified Richardson's constant from here on. At this point we must mention that Richardson's constant is well defined for crystalline materials and depends on the effective mass. However due to the amorphous nature of TiO_x and for the purpose of compact modeling, we empirically assume a temperature dependence on Richardson's constant. Eq. (2) can be rearranged as,

$$\ln(I) = \ln(AA_m^{*}T^{C_T}) - \frac{q\phi_B}{k_B T} + \frac{q\alpha\sqrt{V}}{k_B T} \tag{3}$$

and let us now consider,

$$A' = \ln\left(AA_m^{*}T^{C_T}\right) - \frac{q\phi_B}{k_B T} \tag{4}$$

then,

$$\ln(I) = A' + \frac{q\alpha\sqrt{V}}{k_B T} \tag{5}$$

Eq. (5) is used to fit I-V characteristics at each temperature in the measured range to obtain $A'(T)$ and $\alpha(T)$. Modified Richardson's constant A_m^* and Schottky barrier height ϕ_B are obtained by fitting eq. (4). And various non-idealities originating from temperature dependence of electric permittivity [20], temperature dependence of the barrier height, other non-idealities due to the film quality and resistance drift etc. can be effectively taken into account in the temperature dependence of α. And to model the temperature dependence of α, any suitable function can be used, however for the devices used in this study we find that, α dependence on temperature can be described as:

$$\alpha(T) = \alpha_2 T^2 + \alpha_1 T + \alpha_0 \tag{6}$$

Beginning from the Schottky current equation eq. (1) and modifying it, we developed a physics based compact model which can accurately describe I-V characteristics in the non-switching regime. The model introduces fitting parameters A_m^*, ϕ_B, C_T, α_0, α_1 and α_2. At the end of this section we would like to note that, the Schottky equations (eq. (1) and (2)) described above are valid only in the non-switching regime and are not intended to describe what occurs within the device during programming, where much higher voltages prevail, nevertheless, since the read voltages are well within the non-switching regime and device resistance is always measured at read voltage (there is a read-out pulse between the two programming pulses in the switching bias), we can still use the Schottky equation to link switching dynamics characteristics measured at different temperatures which is explained in the next section.

IV. Temperature dependence in the switching dynamics model

In the previous part of the series we have proposed a physics-agnostic empirical model for switching dynamics. The key equations are restated here to maintain the reading continuity. The initial state-referred resistance is defined as,

$$\Delta R = R - R_0 \tag{7}$$

where R_0 is the resistance value of the memristor before the application of a switching bias. The change in the ΔR at n[th] pulse is given by,

$$\Delta R_n = -R_p \ln\left(\frac{-st_w}{R_p}+1\right), \text{ for } n=1$$
$$\Delta R_n = -R_p \ln\left(\frac{-st_w}{R_p}+\exp\left(\frac{-\Delta R_{n-1}}{R_p}\right)\right), \text{ for } n>1 \tag{8}$$

where t_w is the pulse width and s and R_p are the fitting parameters. For the very first pulse in the switching bias $\Delta R_0 = 0$.

In contrast, the temperature dependence in the physics-based model begins from the modified Schottky equation. Eq. (2) implies that the resistance of the memristor can be calculated as:

$$R = \frac{V_r}{AA_m^* T^{C_T}} \exp\left(\frac{q(\phi_B - \alpha\sqrt{V_r})}{k_B T}\right) \tag{9}$$

where, V_r is the read voltage which is typically chosen in the non-switching regime and throughout this study we use it to be 200 mV. Using eq. (2) to take a temperature ratio we obtain:

$$\frac{R(T_2)}{R(T_1)} = \left(\frac{T_1}{T_2}\right)^{C_T} \exp\left(\frac{q(\phi_B - \alpha\sqrt{V_r})(T_1-T_2)}{k_B T_1 T_2}\right) \tag{10}$$
$$= \kappa(T_1, T_2) \tag{11}$$

where $\kappa(T_1, T_2)$ is a function typical to the Schottky emission conduction mechanism. In the next section, from the PRT data, we will show that, irrespective of the pulse number, the measured resistance ratio $R(T_2)/R(T_1)$ always follows this typical $\kappa(T_1, T_2)$ characteristic. Now, from eq. (7), (8) and (11), and dropping the (T_1, T_2) argument of κ for convenience we can write:

$$R_n(T_2) = \kappa R_0(T_1) \tag{12}$$
$$-\kappa R_p(T_1) \ln\left(\frac{-\kappa s(T_1) t_w}{\kappa R_p(T_1)} + \exp\left(\frac{\kappa(R_{n-1}(T_1) - R_0(T_1))}{\kappa R_p(T_1)}\right)\right)$$

which allows us to predict $R(T_x)$ for any temperature within the valid range of the approximation, so long as we know $R(T_y)$ for some temperature T_y within said range.

This links with our empirical formulation of the model from part I of the series. Specifically, we can compare eq. (12) and eq. (8) in order to infer:

$$s(T_2) = \kappa(T_1, T_2) s(T_1) \tag{13}$$
$$R_p(T_2) = \kappa(T_1, T_2) R_p(T_1) \tag{14}$$

Eq. (13) and eq. (14) essentially state that the device resistance and the switching dynamics model parameters are scaled down/up according to the Schottky current equation temperature scaling factor κ, which then needs to be tested by experiment.

V. Results and Discussion

Fig. 2(a) and (b) show the I-V characteristics of Pt/TiO_x/Pt memristor (memristor I-b) in the first and third quadrants in log and linear scales respectively. Since we use a small positive voltage as a read out voltage which falls in the first quadrant, likewise a third quadrant read-out voltage can also be chosen.

parameter	first quadrant value	third quadrant value	units
$q\phi_B$	0.277	0.279	eV
A_m^*	0.002386	0.002675	A/(K^{2}cm^2)
C_T	2.0	2.0	
α_2	-5.261×10^{-6}	-4.265×10^{-6}	($\sqrt{\text{V}}$/K^2)
α_1	3.288×10^{-3}	2.542×10^{-3}	($\sqrt{\text{V}}/K$)
α_0	-2.643×10^{-1}	-1.456×10^{-1}	($\sqrt{\text{V}}$)

TABLE I
Parameters of modified Schottky model used to describe the I-V behaviour of our test device in the non-invasive regime.

Fig. 2(a) and (b) also show the model fits to the measured I-V characteristics. Fig. 2(c) and (d) show the values of A' and α at different temperatures which are obtained by fitting eq. (5) to the data. Next, By fitting eq. (4) we obtain the values of C_T, A_m^* and ϕ_B. Temperature dependence of α for this particular memristor is described using second order polynomial (eq. (6)). Table I presents the extracted model parameters and Fig. 2(c) and (d) show the corresponding equation fits. From Fig. 2(a) and (b), it can be seen that the physics-based static I-V compact model can accurately describe the I-V characteristics of the memristor in the non-switching regime.

We now discuss the switching dynamics of the memristor I-b. Fig. 3(a) show the PRT data of ΔR at 313 K and the corresponding train of pulses of the switching bias is shown in Fig. 3(b). The alternate polarity sequence of switching biases of magnitudes 0.84 V to 1.16 V with step size of 0.04 V is used to obtain the PRT characteristics. The switching dynamics model described in eq. (8) is fitted to extract the model parameters s and R_p. Fig. 3(c) and (d) show the extracted values of s and R_p at different bias values. The bias dependence of s and R_p is approximated by exponential expressions.

$$s = A_s \exp\left(V/V_{0,s}\right) \tag{15}$$
$$R_p = A_{R_p} \exp\left(V/V_{0,R_P}\right) \tag{16}$$

The switching dynamics modeling methodology up to this point is identical to that of part I of this series except that PRT data is fitted at only one temperature (313 K in this case). In the next step of the methodology we adopt a physics-based approach and use eqs. (11)-(14) in order to derive (and model) the temperature dependence of switching dynamics model parameters from the static I-V equations.

Measured results, shown in Fig. 4(a), illustrate the PRT data of the memristor obtained at temperatures 313 K - 353 K. Fig. 4(b) presents ratios of resistance at various temperatures vs a baseline value taken at 313 K. The ratios are taken for resistance values measured at the end of the first, middle and the last pulse of the each switching bias in the PRT measurement experiment. The figure also presents the ratios predicted by eq. (11) i.e. from the fitted static I-V model. It can be seen that, irrespective of the pulse number and the amplitude of the switching bias, experimentally determined ratios closely follow the theoretical predictions. Using eq. (11), (13) and (14) values of s and R_p at elevated temperatures can indeed be predicted. The corresponding switching dynamics characteristics obtained from the predicted values of s and R_p are overlaid on the PRT data in Fig. 4. The agreement

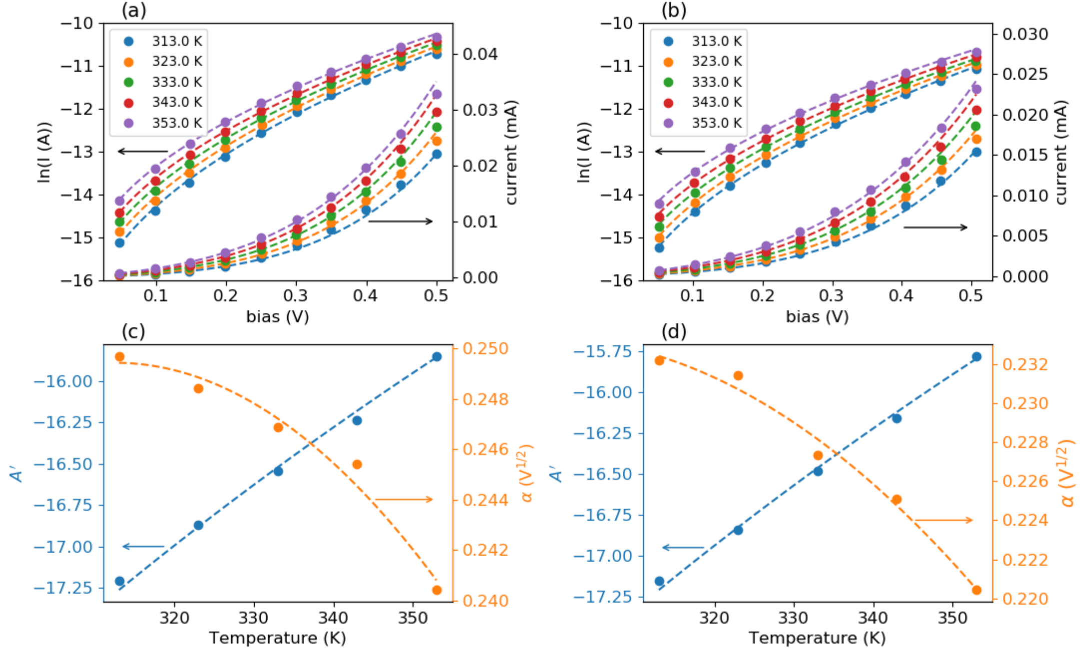

Fig. 2. (a) and (b) are first and third quadrant I-V characteristics respectively of an electroformed Pt/TiO$_x$/Pt memristor (memristor I-b) in log and linear scales. For third quadrant I-V, we have dropped the negative sign in both bias and current. The figures also show the static I-V model fit to the data (dashed lines). (c) and (d) show extracted temperature dependence of A' and α for first and third quadrant I-V fits respectively. For both the quadrants fits eq. (4) is used to fit $A'(T)$ whereas a second order polynomial, eq. (6), is used to fit $\alpha(T)$.

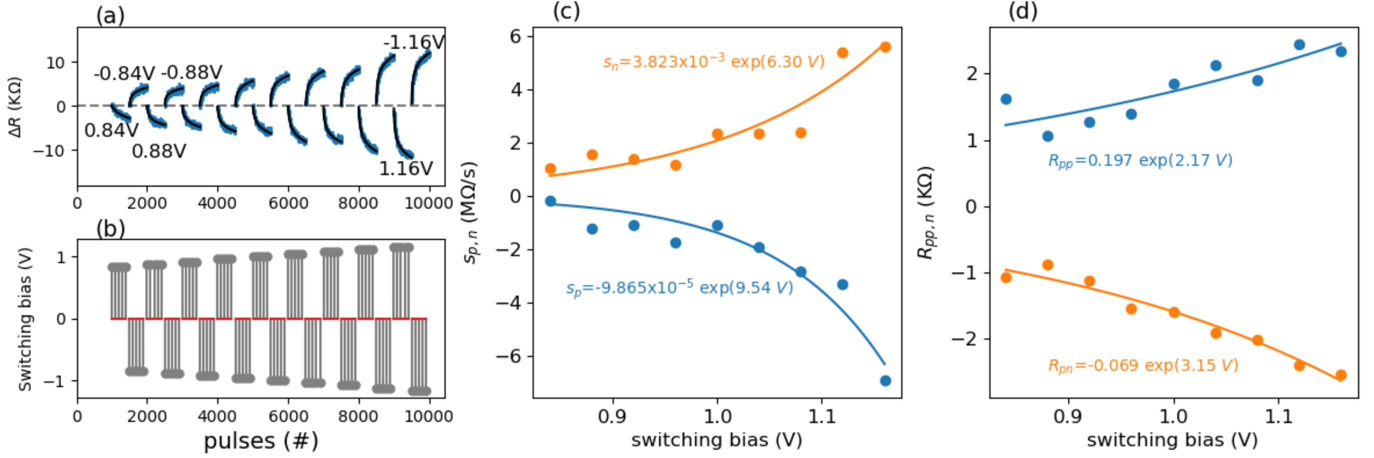

Fig. 3. (a) PRT characteristics of initial state-referred resistance (ΔR) of Pt/TiO$_x$/Pt memristor and the switching model fit using eq. (8). (b) Applied switching bias of alternate polarity. In each switching bias train of 500 pulses with pulse width 100 μs and 10 ms inter-pulse off-time is used. Switching model parameter values obtained by fitting eq. (8) to the data for applied switching bias and corresponding equation fits for (c) parameter s and (d) parameter R_p. Additional subscripts p and n indicate the polarity of the switching bias.

between calculated PRT characteristics and measured data is good everywhere, except at large amplitude switching biases at 343 K and 353 K. The reason for the discrepancy is not clear and further studies are required in that direction. Nevertheless, our proposed physics-based approach presents a direction for obtaining a computationally efficient switching dynamics model which can accommodate range of temperatures (low and elevated) near the room temperature.

We further show that the proposed physics-based model can be applied to another type of TiOx memristor device. We use the PRT measurements data of memristor II mentioned in part I of the series and are presented in Fig. 5(a). We use eq. (10) to obtain $R(T)/R(300K)$ the characteristics shown in Fig. 5(b). Here, we use apparent barrier height defined as $\phi_{B,app} = \phi_B - \alpha\sqrt{V_{read}}$ as a fitting parameter. The visual fit using $q\phi_{B,app}$ = 0.13 eV is also shown in Fig. 5(b). Fig. 5(a) Also shows the PRT characteristics predicted at elevated temperatures.

Fig. 6 shows a comprehensive comparison of model errors for memristor I-b and memristor II. For a fair comparison we

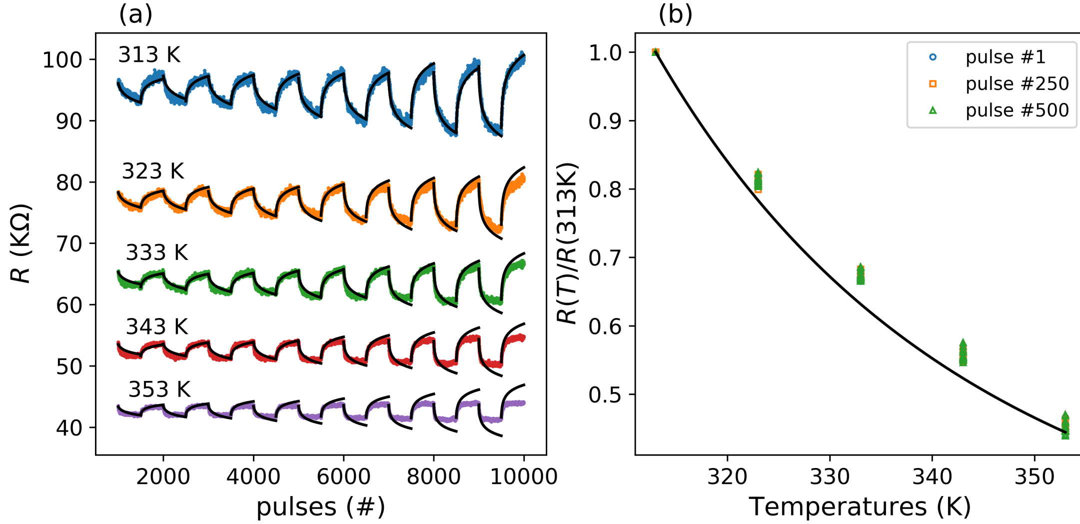

Fig. 4. (a) PRT data of memristor, at a range of temperatures from 313 K to 353 K. It can be observed that the resistance values are decreasing with temperature. This can be easily shown to be the case according to the Schottky current equation (1). It can also be observed that the magnitude of change in resistance is also progressively reduced. (b) Characteristic temperature dependence originating from the Schottky emission based conduction mechanism. Irrespective of pulse number, the ratio of resistances measured at any pair of different temperatures follows the characteristic (solid line) predicted by the Schottky emission mechanism.

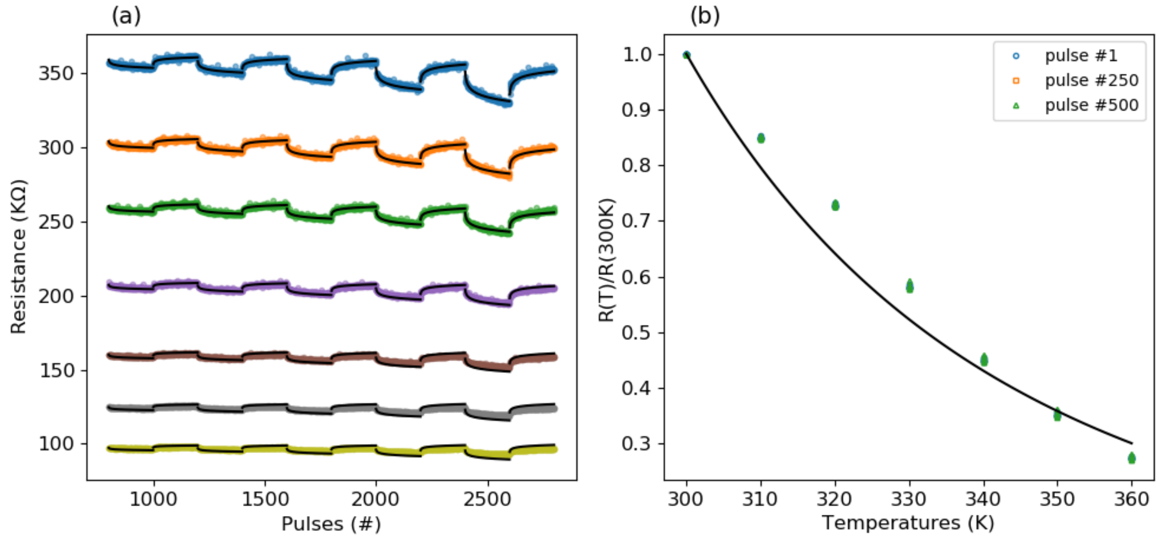

Fig. 5. (a) PRT measurement data of memristor II for temperatures 300 K-360 K. Stage II fitting of PRT characteristics is overlaid for 300 K data whereas for elevated temperatures predicted PRT measurements are overlaid. (b) Characteristics temperature dependence of memristor II exhibit a very similar behaviour to that of the Pt/TiOx/Pt memristor (memristor I-b) characteristics shown in Fig. 4(b).

define the root mean square % error as,

$$\% \text{ RMS error} = \frac{100}{N}\sqrt{\sum_{N}\left(\frac{\Delta R_{data} - \Delta R_{fitted}}{\Delta R_{data}}\right)^2} \quad (17)$$

For the error comparisons we choose $N = 5$ which corresponds to the pulses at the end of each switching bias. Fig. 6(a) and (b) present fitting errors in behavioural modelling (part I of the series) and physics-based modelling (this part). The errors are calculated as mentioned in eq(17) for memristor I-b and memristor II for all temperatures and switching biases. For memristor I-b (Fig. 6(a)), behavioural model exhibit smaller errors at all temperatures and switching biases, whereas errors for physics-based model exhibit significantly large errors at higher temperatures. However, for smaller temperatures, there is no clear criterion on which one model can be chosen over another. A similar observation follows for memristor II. For higher temperatures, physics-based model does exhibit significantly large errors, nevertheless, it does provide a qualitative explanation for the reduction in resistive switching with temperature.

VI. Conclusions

The key conclusion of this paper is experimentally showing that directly applying the Schottky equation-based temperature dependence of subthreshold I-V behaviour to supra-threshold

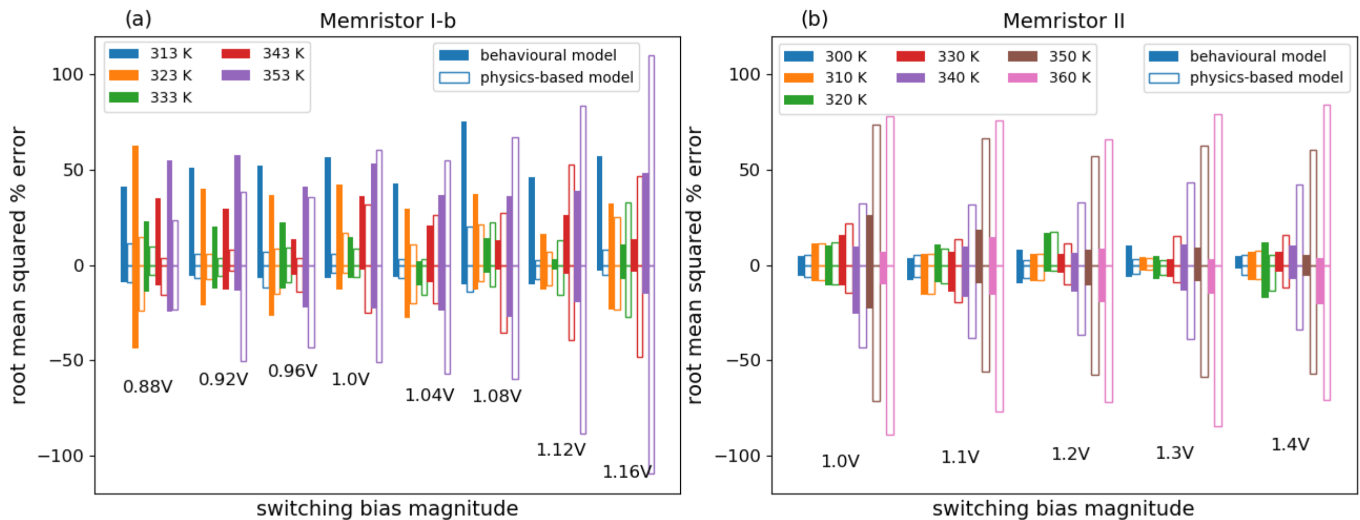

Fig. 6. Root means squared values of percentage error calculated using eq. (17) for each bias and temperatures. Fitting errors are sampled at 5 pulses at the end of each switching bias (N=5) for (a) memristor I-b and (b) for memristor II. In (a) and (b) colour key determines the temperature whereas the other legend key which shows open and coloured bar distinguishes between the model. Coloured bars correspond to the behavioural model (previous part) and open bars correspond to the physics-based model (this part).

switching yields a remarkably accurate prediction of how resistive switching is affected by variations in temperature. Indeed, the magnitude of resistive switching scales down (or up). This work on physics-based model helps to explain this behaviour which is rooted in the Schottky emission as the conduction mechanism which holds at the low voltages (in non-switching regime) typically applied when reading the device. We find that Schottky equation based physics-based model holds for a significant part of the PRT data except at higher switching biases and at higher temperatures. The mismatch at sufficiently elevated temperature conditions is of as yet unknown origin, but we may speculate that beyond a certain degree of invasiveness (high voltage) and at a sufficiently high temperature, thermal effects could begin to appear, which would deviate the trends in fitting parameters $s(T)$ and $R_p(T)$. To this end, further investigation is needed for uncovering memristor behaviour at temperatures outside the range used in this study (and in particular towards higher temperatures) for determining the limits of the present model.

VII. Acknowledgements

This work was supported by FORTE which is a UKRI Engineering and Physical Sciences Research Council Programme Grant EP/R024642/1.

VIII. Supplementary Material

All the data and scripts supporting this study are available at University of Southampton repository at

References

[1] D. B. Strukov, G. S. Snider, D. R. Stewart, and R. S. Williams, “The missing memristor found,” Nature, vol. 453, pp. 80 EP –, May 2008. [Online]. Available: https://doi.org/10.1038/nature06932

[2] N. Gergel-Hackett, B. Hamadani, B. Dunlap, J. Suehle, C. Richter, C. Hacker, and D. Gundlach, “A flexible solution-processed memristor,” IEEE Electron Device Letters, vol. 30, no. 7, pp. 706–708, June 2009. [Online]. Available: https://doi.org/10.1109/LED.2009.2021418

[3] A. Serb, J. Bill, A. Khiat, R. Berdan, R. Legenstein, and T. Prodromakis, “Unsupervised learning in probabilistic neural networks with multi-state metal-oxide memristive synapses,” Nature Communications, vol. 7, no. 1, p. 12611, September 2016. [Online]. Available: https://doi.org/10.1038/ncomms12611

[4] I. Gupta, A. Serb, A. Khiat, R. Zeitler, S. Vassanelli, and T. Prodromakis, “Real-time encoding and compression of neuronal spikes by metal-oxide memristors,” Nature Communications, vol. 7, no. 1, p. 12805, September 2016. [Online]. Available: https://doi.org/10.1038/ncomms12805

[5] J. J. Yang, M. D. Pickett, X. Li, D. A. A. Ohlberg, D. R. Stewart, and R. S. Williams, “Memristive switching mechanism for metal/oxide/metal nanodevices,” Nature Nanotechnology, vol. 3, no. 7, pp. 429–433, June 2008. [Online]. Available: https://www.nature.com/articles/nnano.2008.160

[6] J. Park, M. Kwak, K. Moon, J. Woo, D. Lee, and H. Hwang, “Tiox-based rram synapse with 64-levels of conductance and symmetric conductance change by adopting a hybrid pulse scheme for neuromorphic computing,” IEEE Electron Device Letters, vol. 37, no. 12, pp. 1559–1562, December 2016. [Online]. Available: https://doi.org/10.1109/LED.2016.2622716

[7] M. J. Kim, I. G. Baek, Y. H. Ha, S. J. Baik, J. H. Kim, D. J. Seong, S. J. Kim, Y. H. Kwon, C. R. Lim, H. K. Park, D. Gilmer, P. Kirsch, R. Jammy, Y. G. Shin, S. Choi, and C. Chung, “Low power operating bipolar tmo reram for sub 10 nm era,” in 2010 International Electron Devices Meeting, December 2010, pp. 19.3.1–19.3.4. [Online]. Available: https://doi.org/10.1109/IEDM.2010.5703391

[8] A. Khiat, P. Ayliffe, and T. Prodromakis, “High density crossbar arrays with sub- 15 nm single cells via liftoff process only,” Scientific Reports, vol. 6, no. 1, p. 32614, 2016. [Online]. Available: https://doi.org/10.1038/srep32614

[9] H. Kim, H. Nili, M. Mahmoodi, and D. B. Strukov, “4k-memristor analog-grade passive crossbar circuit,” CoRR, vol. abs/1906.12045, June 2019. [Online]. Available: http://arxiv.org/abs/1906.12045

[10] L. Michalas, S. Stathopoulos, A. Khiat, and T. Prodromakis, “Conduction mechanisms at distinct resistive levels of pt/tio2-x/pt memristors,” Applied Physics Letters, vol. 113, no. 14, p. 143503, October 2018. [Online]. Available: https://doi.org/10.1063/1.5040936

[11] J. G. Simmons, “Generalized formula for the electric tunnel effect between similar electrodes separated by a thin insulating film,” Journal of Applied Physics, vol. 34, no. 6, pp. 1793–1803, June 1963. [Online]. Available: https://doi.org/10.1063/1.1702682

[12] S. Kvatinsky, M. Ramadan, E. G. Friedman, and A. Kolodny, “Vteam: A general model for voltage-controlled memristors,” IEEE Transactions on Circuits and Systems II: Express Briefs, vol. 62, no. 8, pp. 786–790, August 2015. [Online]. Available: https://doi.org/10.1109/TCSII.2015.2433536

[13] I. Messaris, A. Serb, S. Stathopoulos, A. Khiat, S. Nikolaidis,

and T. Prodromakis, “A data-driven verilog-a reram model,” IEEE Transactions on Computer-Aided Design of Integrated Circuits and Systems, vol. 37, no. 12, pp. 3151–3162, December 2018. [Online]. Available: https://doi.org/10.1109/TCAD.2018.2791468

[14] C. Yakopcic, T. M. Taha, G. Subramanyam, and R. E. Pino, “Generalized memristive device spice model and its application in circuit design,” IEEE Transactions on Computer-Aided Design of Integrated Circuits and Systems, vol. 32, no. 8, pp. 1201–1214, Aug 2013. [Online]. Available: https://doi.org/10.1109/TCAD.2013.2252057

[15] M. D. Pickett, D. B. Strukov, J. L. Borghetti, J. J. Yang, G. S. Snider, D. R. Stewart, and R. S. Williams, “Switching dynamics in titanium dioxide memristive devices,” Journal of Applied Physics, vol. 106, no. 7, p. 074508, October 2009. [Online]. Available: https://doi.org/10.1063/1.3236506

[16] L. Michalas, A. Khiat, S. Stathopoulos, and T. Prodromakis, “Electrical characteristics of interfacial barriers at metal—TiO2 contacts,” Journal of Physics D: Applied Physics, vol. 51, no. 42, p. 425101, September 2018. [Online]. Available: https://iopscience.iop.org/article/10.1088/1361-6463/aadbd2

[17] “ArcOne measurement board,” https://www.arc-instruments.co.uk/products/arc-one/.

[18] R. Berdan, A. Serb, A. Khiat, A. Regoutz, C. Papavassiliou, and T. Prodromakis, “A μ -controller-based system for interfacing selectorless rram crossbar arrays,” IEEE Transactions on Electron Devices, vol. 62, no. 7, pp. 2190–2196, July 2015. [Online]. Available: https://doi.org/10.1109/TED.2015.2433676

[19] T. Abbey, A. Serb, N. Vasilakis, L. Michalas, A. Khiat, S. Stathopoulos, and T. Prodromakis, “An embedded environmental control micro-chamber system for rram memristor characterisation,” in 2018 IEEE International Symposium on Circuits and Systems (ISCAS), May 2018, pp. 1–4. [Online]. Available: https://doi.org/10.1109/ISCAS.2018.8351673

[20] J. D. M. N. L. N. MLj Napijalo, Z Nikolic, “Temperature dependence of electric permittivity of linear dielectrics with ionic and polar covalent bonds,” Journal of Physics and Chemistry of Solids, vol. 59, no. 8, pp. 1255–1258, August 1998. [Online]. Available: https://www.sciencedirect.com/science/article/pii/S0022369798000493